Ground-state properties and symmetry energy of neutron-rich and neutron-deficient Mg isotopes

M. K. Gaidarov,[1] P. Sarriguren,[2] A. N. Antonov,[1] and E. Moya de Guerra[3]

[1]*Institute for Nuclear Research and Nuclear Energy, Bulgarian Academy of Sciences, Sofia 1784, Bulgaria*
[2]*Instituto de Estructura de la Materia, IEM-CSIC, Serrano 123, E-28006 Madrid, Spain*
[3]*Grupo de Física Nuclear, Departamento de Física Atómica, Molecular y Nuclear, Facultad de Ciencias Físicas, Unidad Asociada
UCM-CSIC(IEM), Universidad Complutense de Madrid, E-28040 Madrid, Spain*

A comprehensive study of various ground-state properties of neutron-rich and neutron-deficient Mg isotopes with $A = 20$–36 is performed in the framework of the self-consistent deformed Skyrme–Hartree–Fock plus BCS method. The correlation between the skin thickness and the characteristics related with the density dependence of the nuclear symmetry energy is investigated for this isotopic chain following the theoretical approach based on the coherent density fluctuation model and using the Brueckner energy-density functional. The results of the calculations show that the behavior of the nuclear charge radii and the nuclear symmetry energy in the Mg isotopic chain is closely related to the nuclear deformation. We also study, within our theoretical scheme, the emergence of an "island of inversion" at the neutron-rich ^{32}Mg nucleus, which was recently proposed from the analyses of spectroscopic measurements of the ^{32}Mg low-lying energy spectrum and the charge rms radii of all magnesium isotopes in the sd shell.

I. INTRODUCTION

The study of nuclear structure has advanced on the basis of the shell structure associated with the magic numbers. This study, however, has been carried out predominantly for stable nuclei, which are on or near the β-stability line in the nuclear chart and have been explored experimentally. Advances in measurements of unstable nuclei have provided information on exotic nuclei toward the neutron and proton drip lines. Close to them, a large variety of formerly unknown nuclear configurations has been observed. The magic numbers in such exotic systems can be a quite intriguing issue. New magic numbers appear and some others disappear in moving from stable to exotic nuclei in a rather novel manner due to specific components of the nucleon-nucleon interaction (see, for example, Ref. [1]).

Low-lying states of neutron-rich nuclei around the neutron number $N = 20$ attract great interest because the spherical configurations associated with the magic number disappear in the ground states. For ^{32}Mg, from the observed population of the excited 0_2^+ state (found at 1.058 MeV) in the (t,p) reaction on ^{30}Mg, it is suggested [2] that the 0_2^+ state is a spherical state coexisting with the deformed ground state and that their relative energies are inverted at $N = 20$. Very recently, a new signature of an existence of an "island of inversion" [3] has been experimentally tested by measuring the charge radii of all magnesium isotopes in the sd shell at ISOLDE-CERN [4] showing that the borderline of this island lies between ^{30}Mg and ^{31}Mg. The new mass measurements of the exotic nuclides $^{30-34}$Mg have led to a value of 1.10 (3) MeV for the empirical shell gap for ^{32}Mg, which reveals the lowest observed strength of nuclear-shell closure for a nuclide with a conventional magic number [5]. Previously, the Coulomb excitation studies of ^{32}Mg also confirmed the large deformation and pointed out the vanishing of the $N = 20$ shell gap [6]. The concept of island of inversion has been explored, for instance, experimentally also

to isotones with $N = 19$ [7] and complementary information about its extent to at least $N = 22$ for the Ne isotopes was obtained [8].

On the theoretical side, the properties of neutron-rich Mg isotopes have been mainly studied in the framework of the shell model [3,9], as well as within self-consistent mean-field approaches; namely, the Skyrme Hartree–Fock (HF) method with pairing correlations (see, for example, Refs. [10–13]) or the Hartree–Fock–Bogoliubov (HFB) method [14]. The ground-state properties of Mg isotopes from the proton-drip-line nucleus ^{20}Mg to the neutron-drip-line nucleus ^{40}Mg have been calculated by using the nonlinear relativistic mean-field (RMF) model with force parameters NL-SH [15]. The latter predicts well the monotonic increase of the neutron-skin thickness with neutron excess and also provides a good description of the binding energies and the charge rms radii of Mg isotopes. The RMF approach with the same NL-SH parameter set has been applied to calculate the energy levels, the proton occupation probabilities of the $1d_{5/2}$, $2s_{1/2}$, and $1d_{3/2}$ states for the even-even nuclei $^{26-40}$Mg, as well as their charge density distributions [16]. It was shown that the level inversion of $2s_{1/2}$ and $1d_{3/2}$ states that may occur for the magnesium isotopes with more neutrons away from the stability line can lead to a large measurable central charge depletion to the charge density distributions for the neutron-rich Mg isotopes. Recently, the constrained HFB plus local quasiparticle RPA method has been used to describe a variety of quadrupole collective phenomena in a unified way, particularly the shape fluctuations in the ground and excited 0^+ states of ^{30}Mg and ^{32}Mg nuclei [17]. The quadrupole deformation properties of the ground and low-lying excited states of the even-even magnesium isotopes with N ranging from 8 to 28 were successfully described in Ref. [18], where an angular-momentum projected generator coordinate method with the Gogny force was explored. The fully microscopic antisymmetrized molecular dynamics calculations with the

same Gogny-D1S effective interaction have well reproduced measured ground-state properties (spin parity, total binding energy, one-neutron separation energy, and matter radii) of Mg isotopes [19]. In Ref. [20], the $N = 20$ and $N = 28$ islands of inversion have been shown to merge in the magnesium chain, enclosing all the isotopes between $N = 19$ and $N = 30$, by performing large-scale shell-model calculations for their description.

The nuclear deformation plays an important role to determine the charge and matter radius of the neutron-rich nuclei, in particular for the description of the structure of the Mg isotopes [12,14,15]. A direct link between the inversion of states in the deformed shell model and the change in the quadrupole deformation takes place [21,22]. Nuclear radii carry also important information about shell effects and residual interactions. The recent development of the radioactive ion beam (RIB) facilities has made it possible to search for anomalous-structure effects, such as the halo and skin, that are related with the isotope and isospin dependencies of the radii. Suzuki *et al.* [23] reported experimental effective rms matter radii of some Na and Mg nuclei. They concluded that the increase of the rms matter radius is mainly due to an increase of the rms neutron radius. The presence of a neutron skin was predicted in heavy Na and Mg nuclei.

The systematic investigations of the nuclear-size properties provide an important information about the saturation property of atomic nuclei. In particular, the neutron-skin thickness as a good isovector indicator [24] has attracted much interest. In Ref. [25] the formation of a neutron skin, which manifests itself in an excess of neutrons at distances larger than the radius of the proton distribution, was analyzed in terms of various definitions. The results obtained are illustrative for the range of the skin sizes to be expected depending on the adopted skin definition. The knowledge of skin thickness gives more insight into the properties of neutron-rich nuclei and allows us to resolve some of the basic features of the equation of state (EOS) of asymmetric nuclear matter (ANM). The neutron-skin thickness is strongly correlated with the density dependence of the neutron-matter EOS [26,27] and of the symmetry energy of nuclear matter (see, e.g., the articles in the topical issue [28]). The precise knowledge of these relationships is essential for predicting the structure of neutron stars; particularly their radii [29].

In our recent works we have studied the relationship between the neutron-skin thickness and some nuclear-matter properties in finite nuclei, such as the symmetry energy at the saturation point s, symmetry pressure p_0 (proportional to the slope of the bulk symmetry energy), and asymmetric compressibility ΔK, for chains of medium-heavy and heavy spherical Ni ($A = 74$–84), Sn ($A = 124$–152), and Pb ($A = 202$–214) nuclei [30] and deformed Kr ($A = 82$–120) and Sm ($A = 140$–156) isotopes [31]. Most of these nuclei are far from the stability line and are of interest for future measurements with radioactive exotic beams. For this purpose, a theoretical approach to the nuclear many-body problem combining the deformed HF + BCS method with Skyrme-type density-dependent effective interactions [32] and the coherent density fluctuation model (CDFM) [33,34] has been used to study nuclear properties of finite nuclei. The analysis of the latter has

been carried out on the basis of the Brueckner energy-density functional (EDF) for infinite nuclear matter [35,36]. It has to be mentioned that the microscopic theoretical approach used is capable of predicting important nuclear matter quantities in neutron-rich exotic nuclei and their relation to surface properties of these nuclei, which is confirmed by the good agreement achieved with other theoretical predictions and some experimentally extracted ground-state properties.

In the light of the new precise spectroscopic measurements of the neutron-rich ^{32}Mg nucleus, which lies in the much explored island of inversion at $N = 20$, in the present work we aim to perform a systematic study of the nuclear ground-state properties of neutron-rich and neutron-deficient Mg isotopes with $A = 20$–36, such as charge and matter rms radii, two-neutron separation energies, neutron, proton, and charge-density distributions, neutron (proton) rms radii and related with them thickness of the neutron (proton) skins. The new data for the charge rms radii [4] is a challenging issue to test the applicability of the mean-field description to light nuclei, thus expecting to understand in more detail the nuclear structure revealed by them. The need of information for the symmetry energy in finite nuclei, even theoretically obtained, is a major issue because it allows one to constrain the bulk and surface properties of the nuclear EDFs quite effectively. Therefore, following our recent works [30,31] we analyze the correlation between the skin thickness and the characteristics related to the density dependence of the nuclear symmetry energy for the same Mg isotopic chain. Such an analysis may probe the accurate account for the effects of interactions in our method within the considered Mg chain, where the breakdown of the shell model could be revealed also by the nuclear symmetry energy changes. Special attention is paid to the neutron-rich ^{32}Mg nucleus by performing additional calculations modifying the spin-orbit strength of the effective interaction, to check theoretically the possible appearance of the island of inversion at $N = 20$.

The structure of this article is the following: In Sec. II we present briefly the deformed HF + BCS method formalism together with the basic expressions for the considered ground-state properties, as well as the CDFM formalism that provides a way to calculate the symmetry energy in finite nuclei. The numerical results and discussions are presented in Sec. III. We draw the main conclusions of this study in Sec. IV.

II. BRIEF SUMMARY OF FORMALISM

The results of the present work have been obtained from self-consistent deformed Hartree–Fock calculations with density-dependent Skyrme interactions [32] and pairing correlations. Pairing between like nucleons has been included by solving the BCS equations at each iteration with a fixed pairing strength that reproduces the odd-even experimental mass differences [37]. Here we give briefly the basic expressions of the nuclear ground-state properties examined for Mg isotopes, as well as the CDFM scheme to calculate the nuclear symmetry energy in finite nuclei.

We consider in this paper the Skyrme force SLy4 [38]. We also show results obtained from other parametrizations; namely, Sk3 [39] and SGII [40], because they are among the

most extensively used Skyrme forces and are considered as standard references.

The spin-independent proton and neutron densities are given by [25,41]

$$\rho(\vec{R}) = \rho(r,z) = \sum_i 2v_i^2 \rho_i(r,z), \qquad (1)$$

where r and z are the cylindrical coordinates of $\vec{R}$, v_i^2 are the occupation probabilities resulting from the BCS equations and ρ_i are the single-particle densities:

$$\rho_i(\vec{R}) = \rho_i(r,z) = |\Phi_i^+(r,z)|^2 + |\Phi_i^-(r,z)|^2, \qquad (2)$$

with

$$\Phi_i^{\pm}(r,z) = \frac{1}{\sqrt{2\pi}} \sum_{\alpha} \delta_{\Sigma,\pm 1/2} \delta_{\Lambda,\Lambda^{\mp}} C_{\alpha}^i \psi_{n_r}^{\Lambda}(r) \psi_{n_z}(z), \qquad (3)$$

and $\alpha = \{n_r, n_z, \Lambda, \Sigma\}$. In Eq. (3), the functions $\psi_{n_r}^{\Lambda}(r)$ and $\psi_{n_z}(z)$ are expressed by Laguerre and Hermite polynomials:

$$\psi_{n_r}^{\Lambda}(r) = \sqrt{\frac{n_r}{(n_r + \Lambda)!}} \beta_{\perp} \sqrt{2} \eta^{\Lambda/2} e^{-\eta/2} L_{n_r}^{\Lambda}(\eta), \qquad (4)$$

$$\psi_{n_z}(z) = \sqrt{\frac{1}{\sqrt{\pi} 2^{n_z} n_z!}} \beta_z^{1/2} e^{-\xi^2/2} H_{n_z}(\xi), \qquad (5)$$

with

$$\beta_z = (m\omega_z/\hbar)^{1/2}, \quad \beta_{\perp} = (m\omega_{\perp}/\hbar)^{1/2},$$
$$\xi = z\beta_z, \quad \eta = r^2 \beta_{\perp}^2. \qquad (6)$$

The multipole decomposition of the density can be written as [32,41]

$$\rho(r,z) = \sum_{\lambda} \rho_{\lambda}(R) P_{\lambda}(\cos\theta)$$
$$= \rho_0(R) + \rho_2(R) P_2(\cos\theta) + \cdots, \qquad (7)$$

with multipole components λ

$$\rho_{\lambda}(R) = \frac{2\lambda + 1}{2} \int_{-1}^{+1} P_{\lambda}(\cos\theta) \rho(R\cos\theta, R\sin\theta) d(\cos\theta), \qquad (8)$$

and normalization given by

$$\int \rho(\vec{R}) d\vec{R} = X, \quad 4\pi \int R^2 dR \rho_0(R) = X, \qquad (9)$$

with $X = Z$, N for protons and neutrons, respectively.

The mean square radii for protons and neutrons are defined as

$$\langle r_{p,n}^2 \rangle = \frac{\int R^2 \rho_{p,n}(\vec{R}) d\vec{R}}{\int \rho_{p,n}(\vec{R}) d\vec{R}}, \qquad (10)$$

and the rms radii for protons and neutrons are given by

$$r_{p,n} = \langle r_{p,n}^2 \rangle^{1/2}. \qquad (11)$$

The matter rms radius can be obtained by

$$r_m = \sqrt{\frac{N}{A} r_n^2 + \frac{Z}{A} r_p^2}, \qquad (12)$$

where $A = Z + N$ is the mass number. Having the neutron and proton rms radii [Eq. (11)], the neutron-skin thickness is usually estimated as their difference:

$$\Delta R = \langle r_n^2 \rangle^{1/2} - \langle r_p^2 \rangle^{1/2}. \qquad (13)$$

The mean square radius of the charge distribution in a nucleus can be expressed as

$$\langle r_{ch}^2 \rangle = \langle r_p^2 \rangle + \langle r_{ch}^2 \rangle_p + (N/Z) \langle r_{ch}^2 \rangle_n + r_{c.m.}^2 + r_{SO}^2, \qquad (14)$$

where $\langle r_p^2 \rangle$ is the mean square radius of the point proton distribution in the nucleus (10), $\langle r_{ch}^2 \rangle_p$ and $\langle r_{ch}^2 \rangle_n$ are the mean square charge radii of the charge distributions in a proton and a neutron, respectively. $r_{c.m.}^2$ is a small correction due to the center-of-mass motion, which is evaluated by assuming harmonic-oscillator wave functions. The last term r_{SO}^2 is a tiny spin-orbit contribution to the charge density. Correspondingly, we define the charge rms radius

$$r_c = \langle r_{ch}^2 \rangle^{1/2}. \qquad (15)$$

In the present work we calculate the symmetry energy $s(\rho)$ of Mg isotopes on the basis of the corresponding definition for ANM. The quantity $s^{ANM}(\rho)$, which refers to the infinite system and therefore neglects surface effects, is related to the second derivative of the energy per particle $E(\rho,\delta)$ using its Taylor-series expansion in terms of the isospin asymmetry $\delta = (\rho_n - \rho_p)/\rho$, where ρ, ρ_n, and ρ_p are the baryon, neutron, and proton densities, respectively (see, e.g., Refs. [30,31,42,43]):

$$s^{ANM}(\rho) = \frac{1}{2} \frac{\partial^2 E(\rho,\delta)}{\partial \delta^2}\bigg|_{\delta=0} = a_4 + \frac{p_0^{ANM}}{\rho_0^2}(\rho - \rho_0)$$
$$+ \frac{\Delta K^{ANM}}{18\rho_0^2}(\rho - \rho_0)^2 + \cdots. \qquad (16)$$

In Eq. (16) the parameter a_4 is the symmetry energy at equilibrium ($\rho = \rho_0$). In ANM, the pressure p_0^{ANM},

$$p_0^{ANM} = \rho_0^2 \frac{\partial s^{ANM}(\rho)}{\partial \rho}\bigg|_{\rho=\rho_0}, \qquad (17)$$

of the nuclear symmetry energy at ρ_0 governs its density dependence and thus provides important information on the properties of the nuclear symmetry energy at both high and low densities. The slope parameter L^{ANM} is related to the pressure p_0^{ANM} [Eq. (17)] by

$$L^{ANM} = \frac{3p_0^{ANM}}{\rho_0}. \qquad (18)$$

In Refs. [30,31] we calculated the symmetry energy, the pressure, and the curvature for *finite nuclei* applying the coherent density fluctuation model [33,34]. The key ingredient element of the calculations is the weight function that in the case of monotonically decreasing local densities [$d\rho(r)/dr \leqslant 0$] can be obtained by using a known density distribution for a given nucleus:

$$|f(x)|^2 = -\frac{1}{\rho_0(x)} \frac{d\rho(r)}{dr}\bigg|_{r=x}, \qquad (19)$$

where $\rho_0(x) = 3A/(4\pi x^3)$ and with the normalization $\int_0^\infty dx |f(x)|^2 = 1$. In the calculations, for the density distribution $\rho(r)$ needed to obtain the weight function $|f(x)|^2$ [Eq. (19)] we use the monopole term $\rho_0(R)$ in the expansion (7).

It can be shown in the CDFM that, under some approximation, the properties of *finite nuclei* can be calculated by using the corresponding ones for nuclear matter, folding them with the weight function $|f(x)|^2$. Along this line, in the CDFM, the symmetry energy for finite nuclei and, related with it, pressure are obtained as infinite superpositions of the corresponding ANM quantities weighted by $|f(x)|^2$:

$$s = \int_0^\infty dx |f(x)|^2 s^{\text{ANM}}(x), \tag{20}$$

$$p_0 = \int_0^\infty dx |f(x)|^2 p_0^{\text{ANM}}(x). \tag{21}$$

The explicit forms of the ANM quantities $s^{\text{ANM}}(x)$ and $p_0^{\text{ANM}}(x)$ in Eqs. (20) and (21) are defined below. They have to be determined within a chosen method for the description of the ANM characteristics. In the present work, as well as in Refs. [30,31], considering the pieces of nuclear matter with density $\rho_0(x)$, we use for the matrix element $V(x)$ of the nuclear Hamiltonian the corresponding ANM energy from the method of Brueckner *et al.* [35,36]:

$$V(x) = AV_0(x) + V_C - V_{CO}, \tag{22}$$

where

$$V_0(x) = 37.53[(1+\delta)^{5/3} + (1-\delta)^{5/3}]\rho_0^{2/3}(x)$$
$$+ b_1\rho_0(x) + b_2\rho_0^{4/3}(x) + b_3\rho_0^{5/3}(x)$$
$$+ \delta^2[b_4\rho_0(x) + b_5\rho_0^{4/3}(x) + b_6\rho_0^{5/3}(x)], \tag{23}$$

with

$$b_1 = -741.28, \quad b_2 = 1179.89, \quad b_3 = -467.54,$$
$$b_4 = 148.26, \quad b_5 = 372.84, \quad b_6 = -769.57. \tag{24}$$

In Eq. (22), $V_0(x)$ is the energy per particle in nuclear matter (in MeV) accounting for the neutron-proton asymmetry, V_C is the Coulomb energy of protons in a flucton, and V_{CO} is the Coulomb exchange energy. Thus, by using the Brueckner method, the symmetry energy $s^{\text{ANM}}(x)$ and the pressure $p_0^{\text{ANM}}(x)$ for ANM with density $\rho_0(x)$ have the forms

$$s^{\text{ANM}}(x) = 41.7\rho_0^{2/3}(x) + b_4\rho_0(x)$$
$$+ b_5\rho_0^{4/3}(x) + b_6\rho_0^{5/3}(x), \tag{25}$$

$$p_0^{\text{ANM}}(x) = 27.8\rho_0^{5/3}(x) + b_4\rho_0^2(x)$$
$$+ \tfrac{4}{3}b_5\rho_0^{7/3}(x) + \tfrac{5}{3}b_6\rho_0^{8/3}(x). \tag{26}$$

In our approach (see also Refs. [30,31]), Eqs. (25) and (26) are used to calculate the corresponding quantities in finite-nuclei s and p_0 from Eqs. (20) and (21), respectively. We note that, in the limit case when $\rho(r) = \rho_0\Theta(R-r)$ and $|f(x)|^2$ becomes a δ function [see Eq. (19)], Eq. (20) reduces to $s^{\text{ANM}}(\rho_0) = a_4$.

III. RESULTS AND DISCUSSION

A. Ground-state properties

We start our analysis by showing the variation of the binding energy E of all Mg isotopes with $A = 20$–36 as a function of their quadrupole parameter β:

$$\beta = \sqrt{\frac{\pi}{5}} \frac{Q}{A\langle r^2\rangle^{1/2}}, \tag{27}$$

where Q is the mass quadrupole moment and $\langle r^2\rangle^{1/2}$ is the nucleus rms radius. The corresponding potential-energy curves obtained with three different Skyrme forces are given in Fig. 1
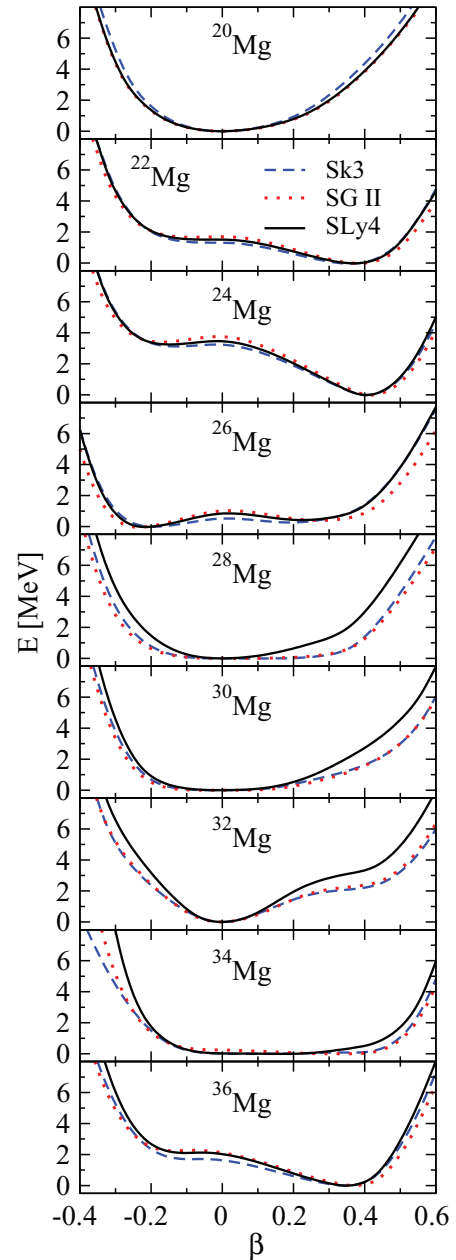

FIG. 1. (Color online) Potential energy curves in even-even Mg isotopes ($A = 20$–36) obtained from HF + BCS calculations with three different Skyrme forces.
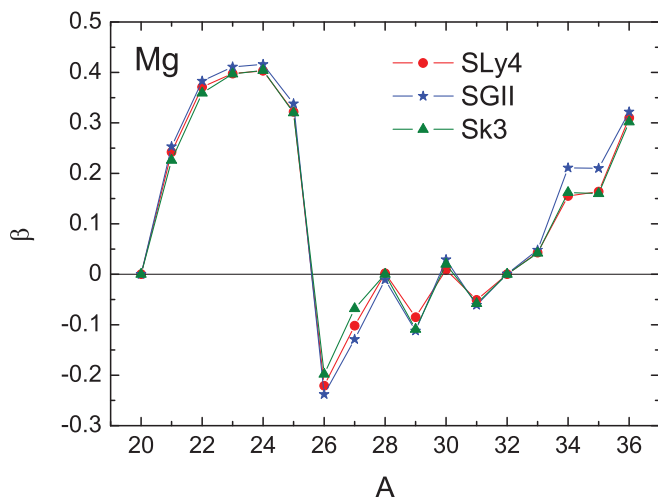
FIG. 2. (Color online) The quadrupole parameter β of the ground state as a function of the mass number A for Mg isotopes ($A = 20$–36) in the cases of SLy4, SGII, and Sk3 forces.

for the even-even isotopes. Similar profiles are obtained by using constant pairing gap parameters in the BCS calculations.

The study of the shape evolution in neutron-rich and neutron-deficient Mg isotopes is further extended by presenting in Fig. 2 the evolution of the quadrupole parameter β of the ground states as a function of the mass number A. A combined analysis of both Figs. 1 and 2 shows that, as expected, the semimagic ^{20}Mg isotope ($N = 8$) is spherical. As the number of neutrons increases we start populating first the $d_{5/2}$ orbital between ^{22}Mg and ^{26}Mg, leading to prolate and oblate deformations in the energy profiles. Prolate shapes with $\beta \sim 0.4$ are ground states in ^{22}Mg and ^{24}Mg, whereas an oblate shape at around $\beta \sim -0.25$ is developed in ^{26}Mg in competition with a prolate shape at around $\beta \sim 0.35$. Due to the conjunction of the $N = Z = 12$ deformed-shell effects, the nucleus ^{24}Mg is the most deformed of the isotopic chain. We obtain rather flat profiles around sphericity in ^{28,30}Mg, whose correct description would need beyond-mean-field techniques involving configuration mixing of the shape fluctuations. ^{32}Mg also becomes spherical, thus showing that the magic number $N = 20$ exists for the ground state of ^{32}Mg in the mean-field theories [15]. For heavier isotopes the prolate deformation grows with the increase of the neutron number for $^{32-36}$Mg. While the prolate solution is only a shoulder in ^{32}Mg at an energy higher than that of the spherical ground state, it becomes already the ground state in ^{34}Mg but practically degenerate with shapes in the range of $-0.15 < \beta < 0.40$. Finally, ^{36}Mg becomes again a well-deformed nucleus with $\beta \sim 0.3$. This situation corresponds to the result obtained in Ref. [21] that the weakly bound neutrons in $^{33-37}$Mg nuclei may prefer to being deformed due to the Jahn–Teller effect. In general, we find almost identical values of the quadrupole parameter β with the three Skyrme parametrizations.

In Fig. 3 we show the proton, neutron, and charge-density distributions of even-even Mg isotopes ($A = 20$–36) calculated with three Skyrme forces. From top to bottom we see the evolution of these densities as we increase the number of neutrons. Starting from the lighter isotope ^{20}Mg we see
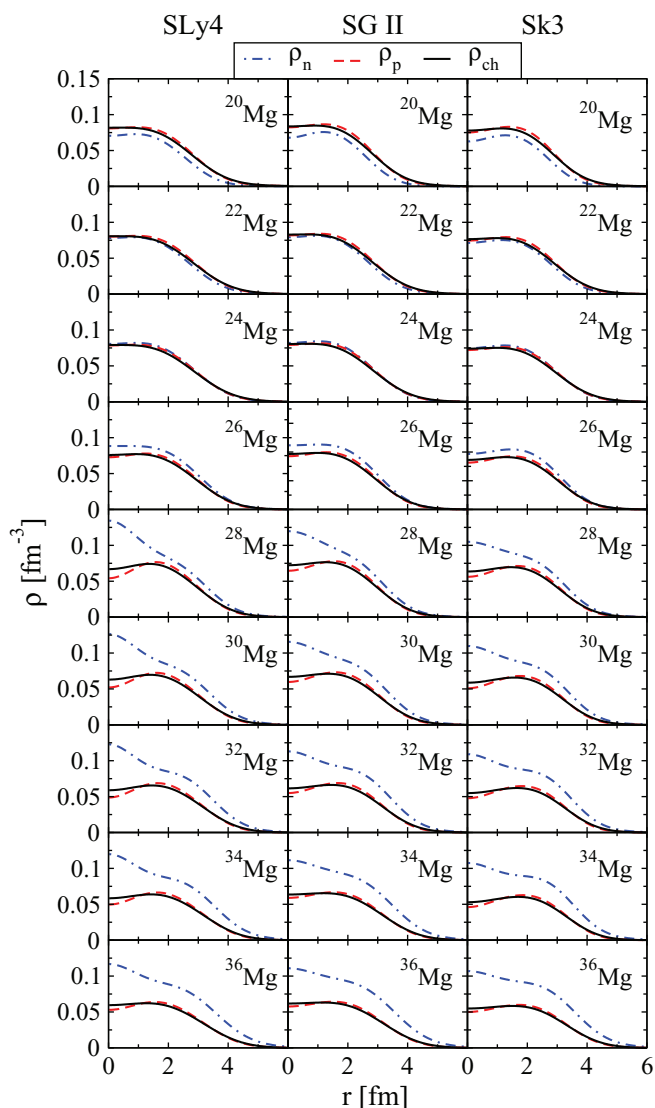

FIG. 3. (Color online) Proton, neutron, and charge-density distributions of even-even Mg isotopes ($A = 20$–36) calculated with SLy4, SGII, and Sk3 interactions.

that the neutron density is clearly below the proton density, because it corresponds to a larger number of protons in that isotope ($Z = 12$, $N = 8$). At the $N = Z = 12$ nucleus ^{24}Mg, we see that both proton and neutron densities are practically the same except for Coulomb effects that make the protons to be a little bit more extended spatially, an effect that has to be compensated with a small depression in the interior of the proton density. The effect of adding more and more neutrons is to populate and extend the neutron densities. The proton distributions try to follow the neutron distributions, thus increasing their spatial extension. This radius enlargement in the case of protons creates a depression in the nuclear interior to preserve the normalization to the constant number of protons, $Z = 12$. It is also worth noting the sudden increase of the neutron density at the origin in ^{28}Mg that corresponds to the filling of the $s_{1/2}$ orbital. The increase of the density in the central region leads to a more compressed nucleus, thus having a smaller radius around this isotope.
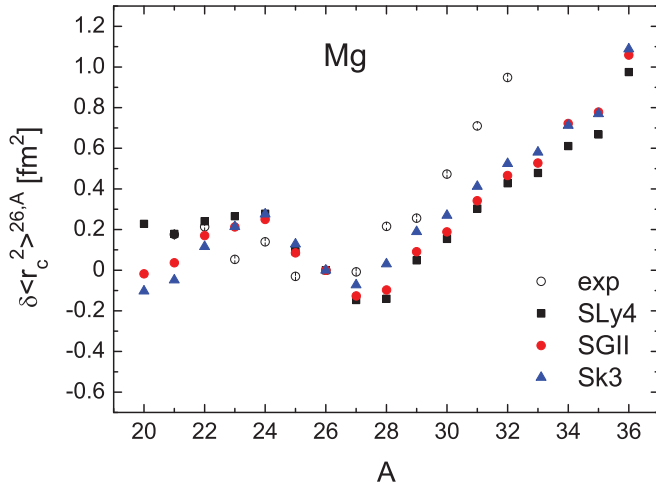
FIG. 4. (Color online) Theoretical (with different Skyrme forces) and experimental [4] isotope shifts $\delta\langle r_c^2\rangle$ of magnesium isotopes relative to ^{26}Mg.

The charge radius is related to the deformation and the isotope shifts of charge radii can be used to investigate the deformations in the isotopic chains. Our results for the squared charge radii differences $\delta\langle r_c^2\rangle^{26,A} = \langle r_c^2\rangle^A - \langle r_c^2\rangle^{26}$ taking the radius of ^{26}Mg as the reference are compared in Fig. 4 with the experimental data [4]. In general, different Skyrme forces do not differ much in their predictions of charge rms radii of magnesium spanning the complete sd shell. The trend of the behavior of the experimental points and theoretical values strongly corresponds to the neutron-shell structure. For $^{21-26}$Mg isotopes, the charge distribution is compressed due to the filling of the $d_{5/2}$ orbital and the charge radii do not fluctuate too much. The addition of more neutrons on either $s_{1/2}$ or $d_{3/2}$ in the range $^{28-30}$Mg results in a fast increase of the radius. Finally, for isotopes beyond ^{30}Mg, where the "island of inversion does exist in terms of the rms charge radius [4], the theoretical results clearly underestimate the experimental points. Obviously, an additional treatment is needed to understand in more detail this specific region. We note the intermediate position of ^{27}Mg, where a minimum is observed in Fig. 4, since one of the neutrons added to ^{25}Mg fills the last $d_{5/2}$ hole and the other neutron populates the $s_{1/2}$ subshell.

The energy gap between nuclear orbitals and the location of nuclear-shell closures is not static but is subject to the proton-to-neutron ratio. An example of experimental observable that probes the location of shell and subshell closures is the two-neutron separation energy S_{2n}. Its trend across isotopic chains provides a fundamental indication for completely filled neutron shells. The two-neutron separation energy can be calculated from the binding energies of neighboring even nuclei $S_{2n} = BE(A,Z) - BE(A-2,Z)$. Results for S_{2n} are plotted in Fig. 5 together with the experimental data [37]. It can be seen that the profile of S_{2n} is rather similar for all Skyrme parametrizations. The results with the SGII force start to deviate from the others at $N > 15$, overestimating the experiment. The general features of the experimental data are satisfactorily reproduced. Especially, the two-neutron separation energy drops at the shell closure $N = 20$ because
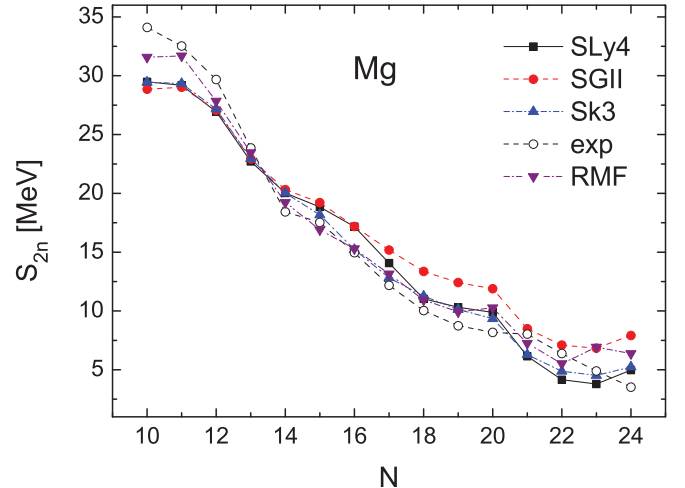

FIG. 5. (Color online) Experimental [37] two-neutron separation energies S_{2n} of Mg isotopes for $A = 20–36$ compared to present calculations (with three Skyrme force parametrizations). Results of RMF calculations are taken from Ref. [15].

neutrons populating orbitals outside closed shells are less bound. This is related to the fact that neutrons in a (nearly) closed neutron shell are more strongly bound and more energy is needed to remove them out of the nuclear medium. Our results for S_{2n} are also in a good agreement with the predictions of the RMF theory with force parameters NL-SH [15].

Figure 6 contains our results with the SLy4, SGII, and Sk3 forces for the neutron and proton mean square radii in the Mg isotopic chain. They are compared with the predictions from RMF theory [15]. We see that the tendency in the radii as a function of the mass number A is quite similar in both approaches, but the proton rms radii with Skyrme are larger than the results from RMF for isotopes heavier than ^{28}Mg. In the case of neutrons, RMF radii are larger than
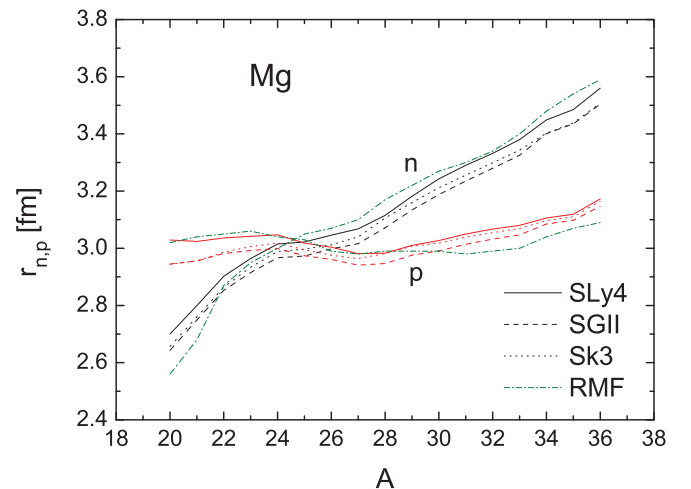

FIG. 6. (Color online) Proton r_p (red curves) and neutron r_n (black curves) rms radii of Mg isotopes calculated by using SLy4, SGII, and Sk3 forces. The results from RMF calculations [15] (green curves) are also given.
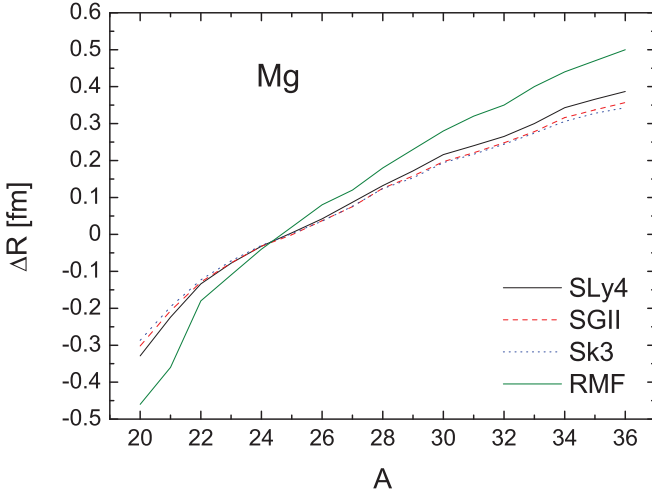
FIG. 7. (Color online) Difference between neutron and proton rms radii Δr_{np} of Mg isotopes calculated by using SLy4, SGII, and Sk3 forces. The RMF-calculation results are from Ref. [15].

FIG. 8. (Color online) Matter r_m rms radii of Mg isotopes ($A = 20$–36) calculated by using SLy4, SGII, and Sk3 forces. The experimental values are taken from Ref. [23]. The results from RMF calculations [15] are also given.

the Skyrme ones for isotopes heavier than ^{24}Mg. As a result we will get systematic differences between the neutron and proton rms radii of isotopes with $A > 24$, which are larger in the case of RMF as compared with the case of Skyrme forces. This is clearly seen in Fig. 7, where we plot the differences between the rms radii of neutrons and protons, $\Delta R = r_n - r_p$. The latter is a simple measure of a neutron (proton) skin emergence in Mg isotopes from the considered isotopic chain. We can see from Fig. 7 that ΔR increases monotonically with neutron excess in the chain of Mg isotopes. Moreover, an irregularity does not seem to be present around ^{32}Mg, neither in the trend of the neutron and proton rms radii (see Fig. 6) nor for their difference. From the Skyrme HF analysis of the rms radii of proton- and neutron-density distributions, Lenske *et al.* [10] have found a proton skin in the neutron-deficient Mg isotopes, while at the neutron dripline the Mg isotopes develop extended neutron skins. It can also be seen from Fig. 7 that, in particular when using SLy4 force, a rather pronounced proton skin in ^{20}Mg develops which exceeds the neutron density by 0.33 fm. The latter value almost coincides with the value of 0.34 fm that has been obtained in Ref. [10] by using a standard Skyrme interaction [44]. In the neutron-rich Mg isotopes our calculations predict quite massive neutron skins whose thickness for ^{36}Mg nucleus reaches 0.39 fm when the same SLy4 parametrization is used. It is known that relativistic models predict rather large neutron radii compared with the nonrelativistic models because the saturation density of asymmetric matter is lower in the EOS when phenomenological nucleon interaction in the RMF theory is used [27,45]. The results shown for neutron radii of Mg isotopes in Fig. 6 and correspondingly for neutron and proton thicknesses in Fig. 7 are consistent with the above general conclusion. The same tendency has been observed in Ref. [25] for Sn, Ni, and Kr isotopes, for which different definitions for the skin thickness were tested in the framework of the same deformed Skyrme HF + BCS model.
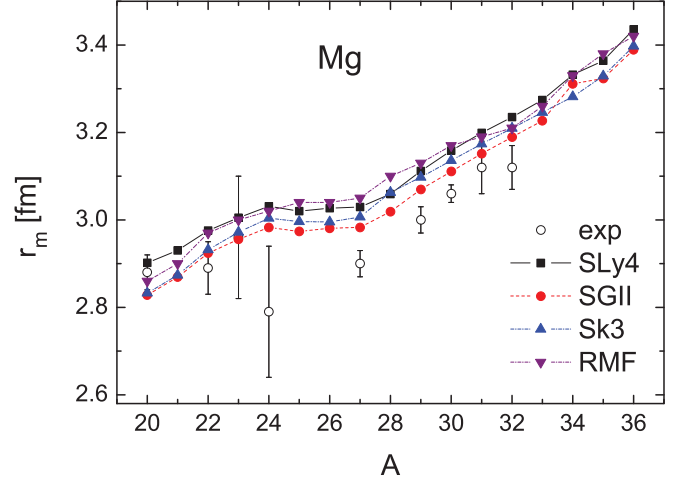
A comparison between the matter rms radii r_m [Eq. (12)] obtained from the Skyrme HF + BCS calculations and their values deduced from the measured interaction cross sections σ_I using a Glauber-type calculation [23] is presented in Fig. 8. The latter were derived by analyzing the data for σ_I for Mg isotopes with use of the Fermi-type distribution under extreme assumptions. Nevertheless, a reasonable agreement is achieved between both theoretical and experimental results for the matter rms radii, as it is seen from the figure. In addition, the RMF predictions for r_m that are also shown in Fig. 8 essentially agree with our results and the data. In general, the growing of the calculated matter rms radii of Mg isotopes follows the same trend, slowly overestimating the experimental data. Due to the large uncertainty of the σ_I result obtained for the stable ^{24}Mg isotope [23], a relatively small value is deduced for its matter radius. The systematic measurements of σ_I, as well as of the total reaction cross sections σ_R, of Mg isotopes on a proton or complex target (see, e.g., Ref. [12] for Mg + ^{12}C cross-section data) may lead to additional information about nuclear deformation through the enhancement of the nuclear size.

Along this line, to better understand the specific neutron shell-model structure leading to a concept of an island of inversion two configurations for ^{32}Mg are displayed in Fig. 9: the closed-shell configuration and the configuration consisting of two neutrons excited from the $1d_{3/2}$ and $2s_{1/2}$ orbitals into the $1f_{7/2}$ and $2p_{3/2}$ orbitals across the $N = 20$ shell gap, making a two-particle, two-hole state. It is well presumed that this promotion of a neutron pair results in a deformed $2p$-$2h$ intruder ground state from the fp shell which competes with the excited (at 1.06 MeV) spherical normal neutron $0p$-$0h$ state of the sd shell.

As is well known, the spin-orbit interaction and the pairing correlations have influence on the deformation of nuclei. Therefore, we perform additional calculations for the ^{32}Mg nucleus by increasing the spin-orbit strength of the SLy4 effective interaction by 20%. Increasing the spin-orbit strength will bring near the neutron $f_{7/2}$ and $d_{3/2}$ orbitals,
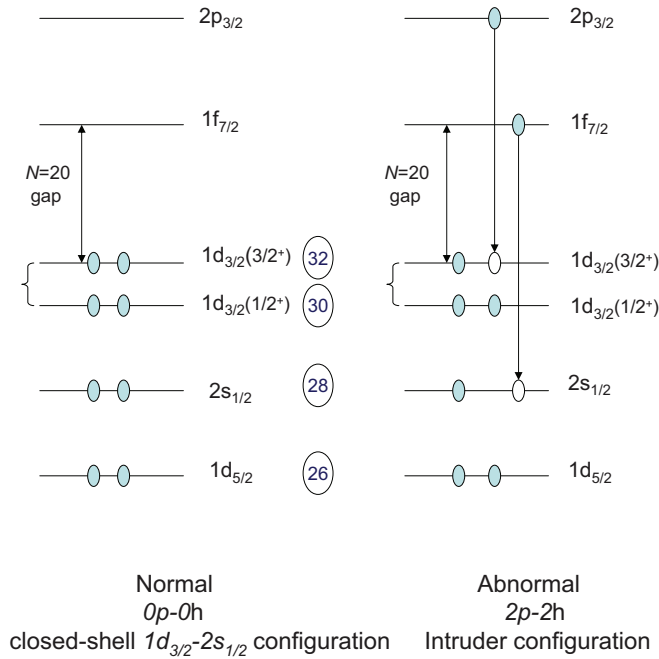
Normal
*0p-0*h
closed-shell $1d_{3/2}$-$2s_{1/2}$ configuration

Abnormal
*2p-2*h
Intruder configuration

FIG. 9. (Color online) The closed-shell and intruder configurations for ^{32}Mg nucleus.

facilitating the promotion of neutrons to the former. According to the Federman and Pittel mechanism [46], protons in the open $d_{5/2}$ orbital overlap substantially with $f_{7/2}$ neutrons ($\ell_p = \ell_n - 1$), generating nuclear deformation by the effect of the isoscalar part of the n-p interaction. The corresponding potential-energy curve is illustrated in Fig. 10 together with the
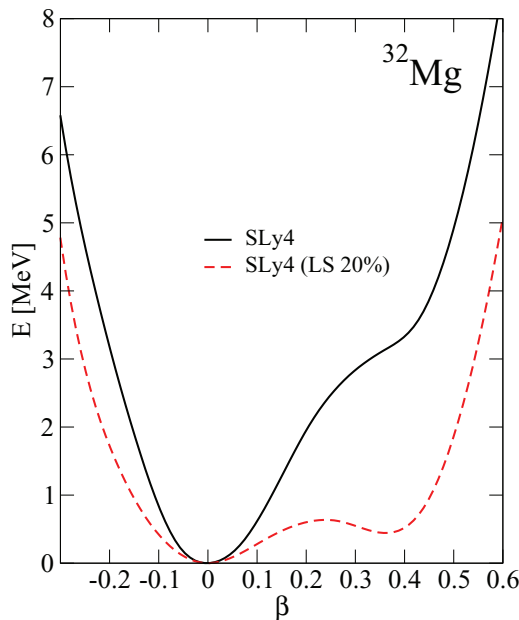

FIG. 10. (Color online) Potential-energy curves of ^{32}Mg obtained from HF + BCS calculations with SLy4 force for the spherical case (black solid line) and in the case when the spin-orbit strength of the effective SLy4 interaction is increased by 20% (red dashed line).
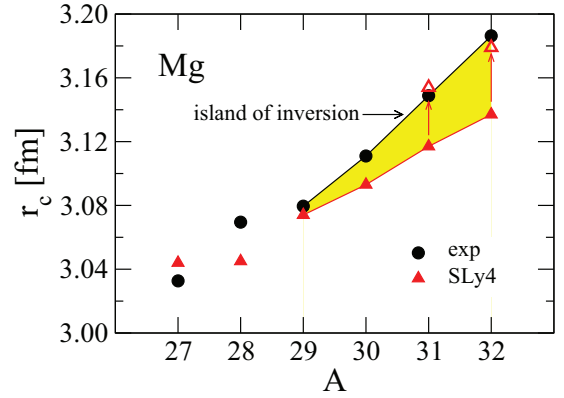

FIG. 11. (Color online) Theoretical (with the SLy4 Skyrme force) and experimental [4] rms charge radii r_c of Mg isotopes in the range $A = 27$–32. The open red triangles represent the calculated values of r_c when the spin-orbit strength of the effective interaction is increased by 20%.

curve from the original SLy4 interaction leading to a spherical equilibrium shape in ^{32}Mg. As a result, we find strong prolate deformation for the intruder configuration ($\beta = 0.38$). This value of the quadrupole deformation is close to the value $\beta = 0.32$ found for the generator coordinate in Ref. [4], where a slight modification of the spin-orbit strength of the effective interaction for a better description of the island of inversion was also applied. Similar effect of the pairing strength on the deformation of ^{32}Mg has been observed in Ref. [15]; namely, that a stronger pairing force of neutrons and a weaker pairing force of protons lead to a larger deformation of the ground state for ^{32}Mg. Thus, the "dual" nature of the latter that is shown in Fig. 9 and that reflects the shape coexistence in ^{32}Mg is in favor to understand the structure of ^{32}Mg.

The impact of these new modified calculations on the evolution of the charge radii, especially in the region of the Mg isotopic chain where an island of inversion is expected, is illustrated in Fig. 11. In addition to ^{32}Mg, we apply the same procedure also to ^{31}Mg nucleus in order to establish better the border of the island. A further increase of the charge radii of these isotopes is found. For ^{31}Mg the charge rms radius increases from 3.117 to 3.154 fm and for ^{32}Mg from 3.137 to 3.179 fm toward the experimentally extracted values for both nuclei indicated in Fig. 11. In general, it can be seen from Fig. 11 that the comparison between the new values that are very close to the experimental data [4] and the previously obtained values of the charge radii of ^{31,32}Mg isotopes can define a region associated with the island of inversion which is not seen in the HF + BCS theoretical method by using the original Skyrme force fit to stable nuclei.

B. Nuclear symmetry energy and its density dependence

In this section we present our results for the symmetry energy s and the neutron pressure p_0 in Mg isotopes from the considered isotopic chain by applying the CDFM scheme (see Sec. II), as well as their relationship with the neutron-skin thickness ΔR. The symmetry energy and the pressure are calculated within the CDFM according to Eqs. (20) and (21)
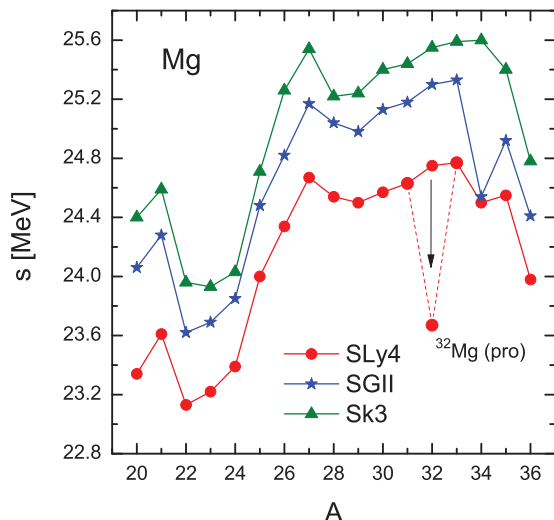
FIG. 12. (Color online) The symmetry energies s for Mg isotopes ($A = 20$–36) calculated with SLy4, SGII, and Sk3 forces.

by using the weight functions (19) calculated from the self-consistent densities in Eq. (1). The differences between the neutron and proton rms radii of these isotopes [Eq. (13)] are obtained from HF + BCS calculations using three different Skyrme forces, SLy4, SGII, and Sk3.

The results for the symmetry energy s [Eq. (20)] as a function of the mass number A for the whole Mg isotopic chain ($A = 20$–36) are presented in Fig. 12. It is seen that the SGII and Sk3 forces yield values of s comparable with each other that lie above the corresponding symmetry-energy values when using SLy4 set. Although the values of s slightly vary within the Mg isotopic chain (23–26 MeV) when using different Skyrme forces, the curves presented in Fig. 12 exhibit the same trend. It is useful to search for possible indications of an island of inversion around $N = 20$ revealed also by the symmetry energy. Therefore, it is interesting to see how the trend of the symmetry energy will be changed when for the magic number $N = 20$ a prolate deformed ground state of ^{32}Mg is obtained (see Fig. 10). We would like to note that, in this case, the modification of the spin-orbit strength of the SLy4 effective interaction by increasing it by 20% leads to a smaller value of $s = 23.67$ MeV compared with the one for the spherical case $s = 24.75$ MeV. Thus, the role of deformation on the nuclear charge radii is also confirmed on the nuclear symmetry energy. Indeed, the results shown in Fig. 12 are related to the evolution of the quadrupole parameter β as a function of the mass number A that is presented in Fig. 2, as well as to the evolution of the charge radii in Fig. 4. We find strong deformations in the range $A = 22$–24 that produce larger charge radii in relation to their neighbors and local wells in the symmetry energy. Next, there is a region of flat energy profiles that correspond to small charge radii and increasing values of the symmetry energy. Above this region we find first spherical shapes that produce a plateau in the symmetry energy from $A = 28$ to $A = 34$ and finally prolate deformations in $A = 36$ that produce very large radii and a sharp decrease in the symmetry energy. This confirms the physical interpretation
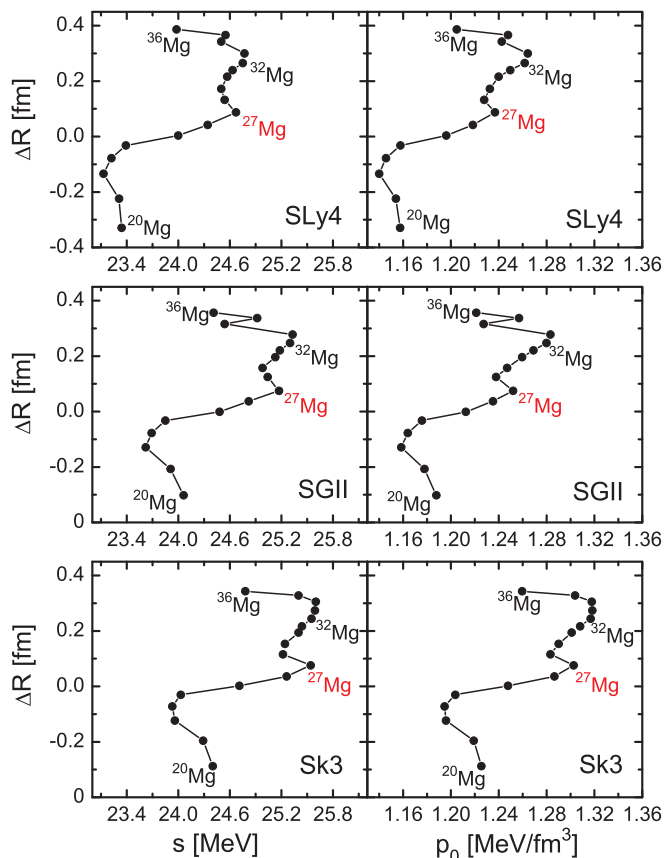

FIG. 13. (Color online) HF + BCS neutron skin thicknesses ΔR for Mg isotopes as a function of the symmetry energy s and the pressure p_0 calculated with SLy4, SGII, and Sk3 forces.

given in Ref. [47], where this fact is shown to result from the moving of the extra neutrons to the surface, thus increasing the surface tension but reducing the symmetry energy. Although the considered Mg chain does not contain a double-magic isotope, it is worth mentioning that we find maximum values within a plateau around the semimagic isotope $A = 32$ that resembles the sharp peak observed in previous works including double-magic nuclei [30,31].

We show in Fig. 13 the correlation of the neutron-skin thickness ΔR [Eq. (13)] of Mg isotopes with the s and p_0 parameters extracted from the density dependence of the symmetry energy around the saturation density. It can be seen from Fig. 13 that, in contrast to the results obtained in Refs. [30,31], there is no linear correlation observed for the Mg isotopic chain. This behavior is valid for the three Skyrme parametrizations used in the calculations. Such a nonlinear correlation of s and p_0 with the neutron-skin thickness ΔR can be explained by the fact that stability patterns are quite irregular within this Mg isotopic chain, where anomalies exist in shell closures around $N = 20$, leading to increased quadrupole collectivity. Additionally, we find the same peculiarity at $A = 27$ from Fig. 4 exhibited in the case of the charge rms radii just reflecting the transition regions between different nuclear shapes of Mg isotopes in the considered chain and a

small change in the behavior for nuclei heavier than ^{32}Mg, as well.

IV. CONCLUSIONS

In this work, we study the nuclear properties of Mg isotopes by means of a theoretical approach to the nuclear many-body problem that combines the coherent density fluctuation model [33,34] and the deformed HF + BCS method (with Skyrme-type density-dependent effective interactions [32]). Three Skyrme parametrizations were involved in the calculations: SLy4, SGII, and Sk3. The CDFM makes the transition from the properties of nuclear matter to the properties of finite nuclei, allowing us to investigate the nuclear symmetry energy s and the neutron pressure p_0 in finite nuclei based on the Brueckner energy-density functional for infinite nuclear matter. The isotopes investigated in this work go from the proton-drip-line nucleus ^{20}Mg up to ^{36}Mg, which approaches the neutron-drip line.

The deformation-energy curves show several transitions of equilibrium shapes as more and more neutrons are added. The lowest isotope ^{20}Mg has an energy minimum at zero deformation parameter, corresponding to the expected equilibrium spherical shape for a semimagic ($N = 8$) nucleus. The next two isotopes, ^{22}Mg and ^{24}Mg, have well-defined prolate equilibrium shapes with deformation parameters around 0.4, while the next one, ^{26}Mg, shows shape coexistence with oblate and prolate equilibrium shapes very close in energy (the oblate minimum being somewhat deeper than the prolate one). As two or four neutrons are added the nucleus becomes soft, with a flat minimum in an extended region around $\beta = 0$, till we reach the next semimagic nucleus ^{32}Mg, which again has spherical equilibrium shape. However, in this new semimagic nucleus one can appreciate a tendency for the nucleus to become prolate, as indicated by the shoulder on the right-hand side of the energy profile. Finally, the nucleus changes again to soft or prolate when adding two (^{34}Mg) or four (^{36}Mg) more neutrons, respectively. Because the proton number is below half-filled-sd shell, the well-defined equilibrium prolate shapes take place when the neutron numbers are either below half sd shell, or below half fp shell. The neutron density profiles are underneath the proton ones when $N < Z$, practically overlapping when $N = Z$, and exceed them when $N > Z$, as expected, showing a sudden strong increase in the central region at $N = 16$. The central bump that appears at this N value is due to the occupancy of the $s_{1/2}$ shell and remains for larger N values. On the other hand, the proton-density profiles tend to develop a central hole with increasing values of A beyond $A = 28$ in order to maintain the proton surface as close as possible to the neutron one. The charge and mass radii follow the trends observed in the experiment, with fluctuating values up to $A = 26$, and smoothly increasing values with A, beyond $A = 27$. These global properties are found to be rather similar with the three Skyrmet forces.

The observed tendency for ^{32}Mg to become deformed has been confirmed by repeating our calculations with SLy4 force modifying slightly the spin-orbit interaction. An increase by 20% of the spin-orbit strength is sufficient to transform the above-mentioned shoulder of the energy profile into a minimum at $\beta = 0.38$, reflecting the role of the intruder fp-shell, mainly the $f_{7/2}$ intruder. The charge radii calculated at the deformed minima obtained with the increased spin-orbit interaction for $A = 31, 32$ are larger (the increase is from 3.117 to 3.154 fm in ^{31}Mg and from 3.137 to 3.179 fm in ^{32}Mg) and are in very good agreement with experiment. Similar effects are caused by slightly changing the proton and neutron pairing strengths. These findings are consistent with results of other theoretical calculations (e.g., within the generator coordinate method) and support the interpretation of this nuclear region as an island of inversion.

The correlations of the the neutron-skin thickness ΔR with the symmetry energy s and with the neutron pressure p_0 do not exhibit linear behavior. They show the same peculiarities at $A = 27$, which reflects the transition regions between different nuclear shapes of Mg isotopes in the considered chain discussed above. The values of the symmetry energy s vary roughly between 23 and 26 MeV, being larger for the Sk3 force, smaller for the SLy4 force, and in between for the SGII effective interaction. Even more dramatic is the considerable change in the trend of symmetry-energy evolution with mass number when we include the results for the prolate ($\beta = 0.38$) ground-state of ^{32}Mg obtained with the spin-orbit-modified SLy4 effective interaction. The behavior of these correlations in this isotopic chain is quite different from that found in our former studies on very heavy isotopic chains, where we found smoother patterns and more regularities. This is clearly due to the fact that shell effects are much more pronounced in these lighter isotopic chains than they are in the heavy ones.

To probe nuclear-structure models it is necessary to have unambiguous experimental observables for the location of shell and subshell closures. Therefore, the study of the nuclear-level inversion and nuclear-bubble phenomenon would be more complete after performing electron scattering off short-lived nuclei on the new generation electron-nucleus RIB facilities. To conclude, we would like to note that further study is necessary to prove theoretically the existence of an island of inversion probed by the REX-ISOLDE experiment. In particular, it is worth performing calculations by including effects of tensor and three-body forces and exploring novel energy-density functionals.

[1] T. Otsuka, R. Fujimoto, Y. Utsuno, B. A. Brown, M. Honma, and T. Mizusaki, Phys. Rev. Lett. **87**, 082502 (2001).

[2] K. Wimmer *et al.*, Phys. Rev. Lett. **105**, 252501 (2010).

[3] E. K. Warburton, J. A. Becker, and B. A. Brown, Phys. Rev. C **41**, 1147 (1990).

[4] D. T. Yordanov *et al.*, Phys. Rev. Lett. **108**, 042504 (2012).

[5] A. Chaudhuri, C. Andreoiu, T. Brunner, U. Chowdhury, S. Ettenauer, A. T. Gallant, G. Gwinner, A. A. Kwiatkowski, A. Lennarz, D. Lunney, T. D. Macdonald, B. E. Schultz, M. C. Simon, V. V. Simon, and J. Dilling, Phys. Rev. C **88**, 054317 (2013).

[6] T. Motobayashi *et al.*, Phys. Lett. B **346**, 9 (1995).

[7] G. Christian *et al.*, Phys. Rev. Lett. **108**, 032501 (2012).

[8] P. Doornenbal *et al.*, Phys. Rev. Lett. **103**, 032501 (2009).

[9] A. Poves and J. Retamosa, Phys. Lett. B **184**, 311 (1987); K. Heyde and J. L. Wood, J. Phys. G **17**, 135 (1991); E. Caurier, F. Nowacki, A. Poves, and J. Retamosa, Phys. Rev. C **58**, 2033 (1998).

[10] H. Lenske and G. Schrieder, Eur. Phys. J. A **2**, 41 (1998).

[11] T. Siiskonen, P. O. Lipas, and J. Rikovska, Phys. Rev. C **60**, 034312 (1999).

[12] W. Horiuchi, T. Inakura, T. Nakatsukasa, and Y. Suzuki, Phys. Rev. C **86**, 024614 (2012).

[13] W. Horiuchi, Y. Suzuki, and T. Inakura, Phys. Rev. C **89**, 011601(R) (2014).

[14] J. Terasaki, H. Flocard, P.-H. Heenen, and P. Bonche, Nucl. Phys. A **621**, 706 (1997).

[15] Z. Ren, Z. Y. Zhu, Y. H. Cai, and G. Xu, Phys. Lett. B **380**, 241 (1996).

[16] Wang Zai-Jun, Ren Zhong-Zhou, and Dong Tie-Kuang, Chin. Phys. C **38**, 024102 (2014).

[17] N. Hinohara, K. Sato, K. Yoshida, T. Nakatsukasa, M. Matsuo, and K. Matsuyanagi, Phys. Rev. C **84**, 061302 (2011).

[18] R. Rodríguez-Guzmán, J. L. Egido, and L. M. Robledo, Nucl. Phys. A **709**, 201 (2002).

[19] S. Watanabe, K. Minomo, M. Shimada, S. Tagami, M. Kimura, M. Takechi, M. Fukuda, D. Nishimura, T. Suzuki, T. Matsumoto, Y. R. Shimizu, and M. Yahiro, Phys. Rev. C **89**, 044610 (2014).

[20] E. Caurier, F. Nowacki, and A. Poves, arXiv:1309.6955.

[21] I. Hamamoto, Phys. Rev. C **76**, 054319 (2007).

[22] D. T. Yordanov, K. Blaum, M. DeRydt, M. Kowalska, R. Neugart, G. Neyens, and I. Hamamoto, Phys. Rev. Lett. **104**, 129201 (2010).

[23] T. Suzuki *et al.*, Nucl. Phys. A **630**, 661 (1998).

[24] P.-G. Reinhard and W. Nazarewicz, Phys. Rev. C **81**, 051303(R) (2010).

[25] P. Sarriguren, M. K. Gaidarov, E. Moya de Guerra, and A. N. Antonov, Phys. Rev. C **76**, 044322 (2007).

[26] B. A. Brown, Phys. Rev. Lett. **85**, 5296 (2000).

[27] S. Typel and B. A. Brown, Phys. Rev. C **64**, 027302 (2001).

[28] B.-A. Li, À. Ramos, G. Verde, and I. Vidaña, Eur. Phys. J. A **50**, 9 (2014).

[29] A. W. Steiner, J. M. Lattimer, and E. F. Brown, Astrophys. J. **722**, 33 (2010); Astrophys. J. Lett. **765**, L5 (2013).

[30] M. K. Gaidarov, A. N. Antonov, P. Sarriguren, and E. Moya de Guerra, Phys. Rev. C **84**, 034316 (2011).

[31] M. K. Gaidarov, A. N. Antonov, P. Sarriguren, and E. Moya de Guerra, Phys. Rev. C **85**, 064319 (2012).

[32] D. Vautherin, Phys. Rev. C **7**, 296 (1973).

[33] A. N. Antonov, V. A. Nikolaev, and I. Zh. Petkov, Bulg. J. Phys. **6**, 151 (1979); Z. Phys. A **297**, 257 (1980); **304**, 239 (1982); Nuovo Cimento A **86**, 23 (1985); A. N. Antonov *et al.*, *ibid.* **102**, 1701 (1989); A. N. Antonov, D. N. Kadrev, and P. E. Hodgson, Phys. Rev. C **50**, 164 (1994).

[34] A. N. Antonov, P. E. Hodgson, and I. Zh. Petkov, *Nucleon Momentum and Density Distributions in Nuclei* (Clarendon Press, Oxford, 1988); *Nucleon Correlations in Nuclei* (Springer-Verlag, Berlin-Heidelberg-New York, 1993).

[35] K. A. Brueckner, J. R. Buchler, S. Jorna, and R. J. Lombard, Phys. Rev. **171**, 1188 (1968).

[36] K. A. Brueckner, J. R. Buchler, R. C. Clark, and R. J. Lombard, Phys. Rev. **181**, 1543 (1969).

[37] G. Audi, A. H. Wapstra, and C. Thibault, Nucl. Phys. A **729**, 337 (2003).

[38] E. Chabanat, P. Bonche, P. Haensel, J. Meyer, and R. Schaeffer, Nucl. Phys. A **635**, 231 (1998).

[39] M. Beiner, H. Flocard, N. Van Giai, and P. Quentin, Nucl. Phys. A **238**, 29 (1975).

[40] N. Van Giai and H. Sagawa, Phys. Lett. B **106**, 379 (1981).

[41] E. Moya de Guerra, P. Sarriguren, J. A. Caballero, M. Casas, and D. W. L. Sprung, Nucl. Phys. A **529**, 68 (1991).

[42] A. E. L. Dieperink, Y. Dewulf, D. Van Neck, M. Waroquier, and V. Rodin, Phys. Rev. C **68**, 064307 (2003).

[43] Lie-Wen Chen, Phys. Rev. C **83**, 044308 (2011).

[44] J. Friedrich and P. G. Reinhard, Phys. Rev. C **33**, 335 (1986).

[45] K. Oyamatsu, I. Tanihata, Y. Sugahara, K. Sumiyoshi, and H. Toki, Nucl. Phys. A **634**, 3 (1998).

[46] P. Federman and S. Pittel, Phys. Rev. C **20**, 820 (1979).

[47] C. J. Horowitz, E. F. Brown, Y. Kim, W. G. Lynch, R. Michaels, A. Ono, J. Piekarewicz, M. B. Tsang, and H. H. Wolter, arXiv:1401.5839.